NEURAL REGENERATION RESEARCH
www.nrronline.org

Research Article

Low-temperature 3D-printed collagen/chitosan scaffolds loaded with exosomes derived from neural stem cells pretreated with insulin growth factor-1 enhance neural regeneration after traumatic brain injury

Xiao-Yin Liu[1, 2, #], Yin-He Feng[3, #], Qing-Bo Feng[4, #], Jian-Yong Zhang[5], Lin Zhong[6], Peng Liu[1], Shan Wang[1], Yan-Ruo Huang[7, *], Xu-Yi Chen[2, 8, *], Liang-Xue Zhou[1, *]

https://doi.org/10.4103/1673-5374.366497
Date of submission: August 18, 2022
Date of decision: November 2, 2022
Date of acceptance: December 2, 2022
Date of web publication: January 5, 2023

From the Contents

Graphical Abstract

Implantation of 3D-CC-INExos improves neural regeneration, ameliorates angiogenesis, and inhibits inflammation and apoptosis in rats after traumatic brain injury (TBI)

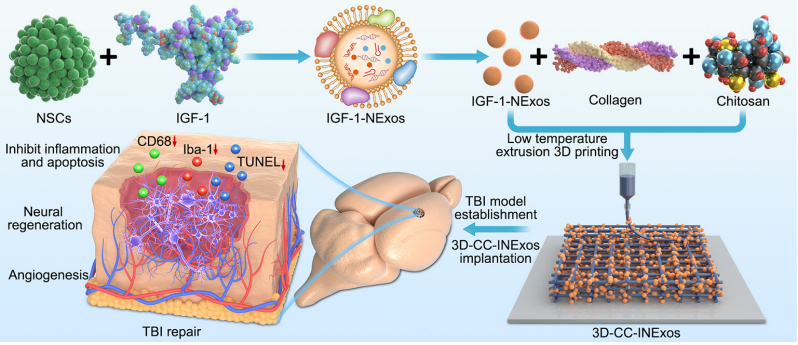

Abstract

There are various clinical treatments for traumatic brain injury, including surgery, drug therapy, and rehabilitation therapy; however, the therapeutic effects are limited. Scaffolds combined with exosomes represent a promising but challenging method for improving the repair of traumatic brain injury. In this study, we determined the ability of a novel 3D-printed collagen/chitosan scaffold loaded with exosomes derived from neural stem cells pretreated with insulin-like growth factor-1 (3D-CC-INExos) to improve traumatic brain injury repair and functional recovery after traumatic brain injury in rats. Composite scaffolds comprising collagen, chitosan, and exosomes derived from neural stem cells pretreated with insulin-like growth factor-1 (INExos) continuously released exosomes for 2 weeks. Transplantation of 3D-CC-INExos scaffolds significantly improved motor and cognitive functions in a rat traumatic brain injury model, as assessed by the Morris water maze test and modified neurological severity scores. In addition, immunofluorescence staining and transmission electron microscopy showed that 3D-CC-INExos implantation significantly improved the recovery of damaged nerve tissue in the injured area. In conclusion, this study suggests that transplanted 3D-CC-INExos scaffolds might provide a potential strategy for the treatment of traumatic brain injury and lay a solid foundation for clinical translation.

Key Words: 3D printing; angiogenesis; chitosan; collagen; exosomes; functional recovery; insulin-like growth factor-1; neural regeneration; neural stem cells; traumatic brain injury

Introduction

Traumatic brain injury (TBI) is a serious health problem worldwide, potentially leading to lifelong disability (Stocchetti et al., 2017; Gao et al., 2020; Wiles, 2022). Despite significant advances in prehospital, perioperative, and intensive care management, TBI continues to cause high mortality and long-term neurological impairment (Wiles, 2022). Specific and effective treatments for TBI, other than preventive measures or intensive care, are limited (Cui et al., 2022), and there is thus an urgent need for improved treatments for TBI. The development of tissue engineering and stem cell therapy may provide new strategies for the treatment of TBI. Biomaterial-based therapies are gaining popularity in experimental applications, including biomolecules, drug delivery, and cell scaffolds, which support the damaged area and also promote tissue regeneration at the injured site (Ma et al., 2019a; Hacene et al., 2022; Verstappen et al., 2022). Biomaterial-based therapies utilizing endogenous neural stem cells (NSCs) for tissue repair may be an alternative strategy to improve neural regeneration in TBI (Tan et al., 2020). NSCs are pluripotent and can mature into different cell types (Jiao et al., 2021). They have been confirmed to promote tissue regeneration and differentiation into oligodendrocytes and promote remyelination (Zipser et al., 2022). NSC therapy thus offers new insights into the treatment of nervous system diseases (Goldman, 2016; Shen et al., 2016). Stem cell transplantation has been recognized as a reliable treatment for many central nervous system diseases in animal models (Hattiangady and Shetty, 2012; Tajiri et al., 2014; Acosta et al., 2015; Goldman, 2016; Gonzalez et al., 2016; Garbuzova-Davis et al., 2017). However, intracranial hemorrhage is a potentially serious complication of stem cell injection using stereotaxic neurosurgery and needle injection, leading to neurological deficits (Shen et al., 2016). Intravenous

[1]Department of Neurosurgery, West China Hospital, West China Medical School, Sichuan University, Chengdu, Sichuan Province, China; [2]Tianjin Key Laboratory of Neurotrauma Repair, Pingjin Hospital Brain Center, Characteristic Medical Center of Chinese People's Armed Police Force, Tianjin, China; [3]Department of Respiratory and Critical Care Medicine, People's Hospital of Deyang City, Affiliated Hospital of Chengdu College of Medicine, Deyang, Sichuan Province, China; [4]Department of Liver Surgery & Liver Transplantation, State Key Laboratory of Biotherapy and Cancer Center, West China Hospital, Sichuan University, Chengdu, Province, China; [5]Department of General Surgery, the Affiliated Hospital of Guizhou Medical University, Guiyang, Guizhou Province, China; [6]The First Affiliated Hospital of Chengdu Medical College, Chengdu, Sichuan Province, China; [7]Department of Anesthesiology, Huashan Hospital, Fudan University, Shanghai, China; [8]Institute of Medical Security for Maritime Rights Protection of Characteristic Medical Center of Chinese People's Armed Police Force, Tianjin, China

***Correspondence to:** Liang-Xue Zhou, MD, zhlxlll@163.com; Xu-Yi Chen, MD, chenxuyi1979@126.com; Yan-Ruo Huang, MD, huangyanruo@126.com.
https://orcid.org/0000-0001-9991-6358 (Liang-Xue Zhou); https://orcid.org/0000-0002-0420-8349 (Xu-Yi Chen); https://orcid.org/0000-0001-7106-590X (Yan-Ruo Huang)
#These authors contributed equally to this paper.

Funding: *This work was supported by the National Major Scientific and Technological Special Project for Significant New Drugs Development, No. 2019ZX09301-147 (to LXZ).*
How to cite this article: *Liu XY, Feng YH, Feng QB, Zhang JY, Zhong L, Liu P, Wang S, Huang YR, Chen XY, Zhou LX (2023) Low-temperature 3D-printed collagen/chitosan scaffolds loaded with exosomes derived from neural stem cells pretreated with insulin growth factor-1 enhance neural regeneration after traumatic brain injury. Neural Regen Res 18(9):1990-1998.*

injection of stem cells is associated with less risk, but most of the injected stem cells are captured by the lung, liver, and spleen, rather than by the injured brain. Magnetic targeting cellular therapy might be another viable stem cell therapy for TBI, resolving the problem of targeting stem cells to the damaged area (Kim et al., 2020; Luo and Du, 2020). However, the low survival rate of NSCs presents another challenge, possibly due to negative effects on the microenvironment in the injured area (Dooley et al., 2014; Othman and Tan, 2020). The above problems mean that NSC therapy is currently not suitable for clinical application.

Exosomes are released by mammalian cells and play essential roles in intercellular communication (Vogel et al., 2018; Sharma et al., 2019). Exosomes signal over short distances within brain tissue and can signal broadly throughout the brain via the cerebrospinal fluid, and have demonstrated biological activity and biological roles in neurons (Vogel et al., 2018). NSC-derived exosomes contain specific micro RNAs (miRNAs) and proteins related to nerve regeneration, neuroprotection, and neuroplasticity (Nakamura et al., 2015; Stevanato et al., 2016; Vogel et al., 2018), and can act as independent metabolic units with positive effects the microenvironment and signaling pathways in normal adult brain (Zhao et al., 2016; Iraci et al., 2017; Vogel et al., 2018). The above advantages suggest that NSC-derived exosomes may be used to treat TBI.

Exosomes produced by pretreating cells with various drugs, cytokines, and physical factors have also demonstrated strong biological activity and function (Hu et al., 2021a). Insulin-like growth factor 1 (IGF-1) is an active protein polypeptide that regulates cellular growth, differentiation, and survival. IGF-1 expressed in brain neurons and glial cells can stimulate the proliferation of neurons and glial precursors and their phenotypic differentiation in the brain (Ayer-le Lievre et al., 1991). A previous study (Ma et al., 2019b) revealed that NSC-derived exosomes pretreated with IGF-1 (IGF-1-Exos, INExos) inhibited the nuclear factor-κB pathway, and that neuroinflammation promoted neuroprotection after spinal cord injury by upregulating miR-219a-2-3p to inhibit the expression of YY1. INExos might thus have excellent reparative effects in TBI.

3D-printing technology allows the creation of personalized scaffolds to match the precise anatomy of the individual, thereby guiding, aligning, and stimulating tissue regeneration. 3D-printed scaffolds combined with stem cell-derived exosomes have been used to promote repair and regeneration of damaged areas in animals with TBI (Chen et al., 2022; Cui et al., 2022; Wang et al., 2022). However, conventional 3D-printing techniques impair the bioactivity of exosomes. We therefore used low-temperature 3D-printed scaffolds incorporating exosomes to maintain the bioactivity of the exosomes. We previously showed that collagen/chitosan might be ideal materials for spinal cord injury repair (Liu et al., 2021). In the current study, we aimed to prepare a novel 3D-printed collagen/chitosan scaffold loaded with exosomes derived from NSCs pretreated with IGF-1 (3D-CC-INExos) and investigated its ability to bridge injured areas and improve neurological functional recovery in rats after TBI. We hypothesized implantation of 3D-CC-INExos improves neural regeneration, ameliorates angiogenesis, and inhibits inflammation and apoptosis in rats after TBI.

Methods

Ethics statement

All animal protocols were reviewed and approved by the Ethics Committee of Sichuan University (approval No. KS2022879; approval date: March 11, 2022) and conducted in strict accordance with international laws and National Institutes of Health policies, including the Guide for the Care and Use of Laboratory Animals (8th ed., National Research Council, 2011).

Isolation and identification of NSCs and NSC-exosomes

NSCs were isolated from the brains of embryonic day 14 (E14) specific-pathogen-free Sprague-Dawley (SD) rats (Chengdu Dossy, Chengdu, Sichuan, China, license No. SCXK (Chuan) 2020-030) and cultured as described previously (Harris et al., 2007; Jiang et al., 2020b). Floating neurospheres were collected by centrifugation (112 × *g* for 5 minutes) and cultured in fresh growth medium. NSCs were purified from neurospheres subcultured to the third generation and identified by nestin markers. Briefly, samples were incubated with primary rabbit anti-nestin monoclonal antibody (1:200; Abcam, Cambridge, UK, Cat# ab105389, RRID: AB_10859398) overnight at 4°C, followed the next day by incubation with secondary antibodies (goat anti-rabbit IgG H&L (Alexa Fluor® 488), 1:1000; Abcam, Cat# ab150077, RRID: AB_2630356) for 1 hour at room temperature. Third-generation NSCs were cultured in two complete media: (1) DMEM/F12 medium (Gibco, Carlsbad, CA, USA) supplemented with 20 ng/mL epidermal growth factor (EGF; PeproTech, Rocky Hill, NJ, USA), 20 ng/mL basic fibroblast growth factor (bFGF; PeproTech), 1× B27 supplement (Gibco), 100 U/mL penicillin (Gibco), and 100 U/mL streptomycin (Gibco); (2) IGF-1 medium (DMEM/F12 medium supplemented with 20 ng/mL EGF, 20 ng/mL bFGF, 1× B27 supplement, 100 ng/mL IGF-1 (PeproTech), 100 U/mL penicillin, and 100 U/mL streptomycin). Exosomes were isolated from NSC supernatant with or without IGF-1 pretreatment by ultracentrifugation, as described previously (Hu et al., 2021b; Zhang et al., 2021c; Han et al., 2022). Briefly, the cell supernatant was centrifuged at 300 × *g* for 10 minutes, 2000 × *g* for 10 minutes, and 10,000 × *g* for 30 minutes at 4°C. The supernatant obtained by gradient centrifugation was centrifuged at 100,000 × *g* for 90 minutes at 4°C to obtain the precipitate, which was resuspended in sterile phosphate-buffered saline (PBS) and centrifuged again at 4°C for 90 minutes at 100,000 × *g*. The resulting precipitate after removal of the supernatant was then resuspended in sterile PBS and stored at –80°C for downstream experiments. The following exosomes were used: NExos (exosomes extracted from supernatant of NSCs cultured in ordinary complete medium) and IGF-1-NExos (INExos; exosomes extracted from supernatant of NSCs cultured in ordinary complete medium supplemented with IGF-1). Exosome morphology was examined by transmission electron microscopy (TEM) (HT7700, Hitachi, Tokyo, Japan). The distribution of exosome size was detected by nanoparticle tracking analysis (NTA) (Malvern Instruments, Malvern, UK) and the expression of the exosome markers CD9 (1:1000; Abcam, Cat# ab236630, RRID: AB_2922400) and CD63 (1:10,000; ProteinTech, Wuhan, Hubei, China, Cat# 67605-1-Ig, RRID: AB_2882811) were assessed by western blotting (WB). The concentration of exosomes was determined using a bicinchoninic acid (BCA) reagent test kit (Beyotime, Shanghai, China).

Preparation of scaffolds

Collagen/chitosan was prepared, as described previously (Liu et al., 2019; Sun et al., 2019). In brief, fresh bovine tendons from the market were crushed thoroughly, placed in 0.05 M Tris buffer, and centrifuged at 3990 × *g* for for 15 minutes to obtain a precipitate. The pellet was dissolved in an acetic acid solution of pepsin and centrifuged to collect the supernatant. The supernatant was added to 3.5 M NaCl solution and stirred well to obtain the salt precipitate, followed by dialysis of the precipitate in deionized water at 4°C for 5 days to obtain the collagen gel. Chitosan (75–85% deacetylation degree; MilliporeSigma, Burlington, MA, USA) was placed in 1% acetic acid solution for full dissolution and subsequent experiments. The collagen/chitosan compound was incubated at 4°C overnight and then divided into four equal parts, as described previously (Liu et al., 2021), and 0.1 g of sterile collagen/chitosan solution was then mixed with a solution containing 200 μg of NSC-derived exosomes (NExos) or 200 μg of IGF-NSC-derived exosomes (INExos) and incubated and stirred for 24 hours at 4°C. The prepared mixed material (collagen/chitosan or collagen/chitosan composite combined with NExos or INExos) was placed in a printer cartridge (Regenovo, Hangzhou, China). The printing process was implemented according to the following parameters: nozzle diameter (160 μm), platform temperature (–20°C), extrusion speed (0.17 mm/min), printing speed (12 mm/s) and layer thickness (0.3 mm). All printed scaffolds were freeze-dried and then cut into a cylinder (diameter 2 mm, height 2 mm) for subsequent animal experiments. Scaffolds were sterilized using ^{60}Co (Huizhou Huada Irradiation Technology Co., Ltd., Huizhou, Guangdong, China) at 4°C for subsequent experiments. Four kinds of scaffolds were used: collagen/chitosan (CC), 3D-printed collagen/chitosan (3D-CC), 3D-printed collagen/chitosan/NExos (3D-CC-NExos), and 3D-printed collagen/chitosan/INExos scaffolds (3D-CC-INExos). Notably, the scaffolds were prepared at low temperature (4°C) to maintain the bioactivity of the exosomes, and the scaffolds were printed at –20°C.

Morphology and degradation of scaffolds *in vivo*

Scaffold morphology was evaluated using a digital camera (D3500, Nikon, Tokyo, Japan), hematoxylin and eosin (HE) staining (Servicebio, Wuhan, Hubei, China), and scanning electron microscopy (Hitachi). The distribution of exosomes was observed following PKH26 labelling under a confocal laser scanning microscope (CLSM, LSM 880, Zeiss, Oberkochen, Germany). The suitable mass ratio of the scaffolds was investigated by manufacturing 3D-CC-INExos scaffolds with five different mass ratios of collagen:chitosan (16:1, 8:1, 1:1, 1:8, 1:16). According to previous *in vivo* scaffold-degradation experiments (Jiang et al., 2020a), three sterile scaffolds (n = 5) with the same mass ratio were implanted into the backs of rats under anesthesia (Intraperitoneal injection of 1% pentobarbital sodium (40 mg/kg, MilliporeSigma)). The initial mass of the scaffold was recorded and the scaffolds with five different masses were removed at 1, 2, 3, 4, 5, 6, 7, and 8 weeks after surgery, to evaluate their degradation. The mass of the scaffold when it was removed was recorded as mass at time (t). The degradation behavior of the scaffold was calculated as: percent mass remaining = mass at time (t)/initial mass × 100. Degradation time curves of the scaffolds were plotted based on the results of the determination.

Physical properties of scaffolds and cumulative exosome release from scaffolds

The water absorption and porosity ratios of the scaffolds were identified by the gravimetric method and volume method, respectively (Sun et al., 2019; Liu et al., 2021). Briefly, water uptake was calculated by immersing each scaffold in PBS for 24 hours. After removing free water from the surface, the sample was weighed (M_t) and the dry weight (M_0) was determined after drying the sample for 2 hours. The water absorption ratio was calculated as: water absorption ratio (%) = $(M_t–M_0)/M_0 \times 100$. To determine porosity, the scaffold was placed in absolute ethanol (volume V_0) for 5 minutes and the volume of alcohol (V_1) was measured after negative pressure degassing until there was no obvious bubble exudation. After removal of the scaffold, the remaining volume of alcohol was measured as V_2 and the porosity ratio was calculated as: porosity ratio (%) = $(V_0–V_2)/(V_1–V_2) \times 100$. The exosome-release characteristics of the CC-INExos and 3D-CC-INExos scaffolds were compared by assessing the cumulative exosome release time by BCA assay (Beyotime) at 1, 3, 5, 7, and 14 days. Based on the results, cumulative release curves of exosomes from the scaffolds were plotted. To prove that scaffold-released exosomes can be endocytosed by NSCs, immunofluorescence staining (IF) was used to assess the localization of the scaffold-released exosomes and NSCs. Scaffold-released exosomes were labeled with PKH26 (MilliporeSigma), and the cytoskeleton of NSCs was labelled with F-Actin-Tracker Green (Beyotime).

Histocompatibility of scaffolds *in vitro* and *in vivo*

To verify the compatibility of the scaffold with NSCs *in vitro*, NSCs were cocultured with scaffolds at a density of 1×10^6/mL and the adhesion rate of NSCs cocultured with the scaffolds was observed at 1, 12, 24, 36, 48, 60, and 72 hours (Liu et al., 2021). The cell adhesion rate was calculated as: cell adhesion rate (%) = number of adherent cells/number of seeded cells × 100. The proliferative capacity of NSCs cocultured with the scaffolds was examined at 1, 3, 5, and 7 days and the viability of NSCs during coculture was assessed by CCK-8 assay (MilliporeSigma), according to the manufacturer's instructions. In brief, CCK-8 solution was added into a 12-well plate of NSCs cocultured with scaffolds at a ratio of 1:10 for 4 hours, and the absorbance of the solution was then measured with a microplate reader (BioTek, Covina, CA, USA) at a wavelength of 450 nm. After coculture for 7 days, the NSC cytoskeleton was visualized by Actin-Tracker Green staining. We then evaluated the differentiation of NSCs cocultured with two different scaffolds after 7 days using IF. Cocultured samples were incubated with the following rabbit primary antibodies: NF (a neurofilament marker; 1:50; Abcam, Cat# ab223343, RRID: AB_2891198), growth-associated protein-43 (GAP43; an axon marker; 1:200; Abcam, Cat# ab75810, RRID: AB_1310252), neuronal nuclear protein (NeuN; a neuron nuclei marker; 1:500; Abcam, Cat# ab177487, RRID: AB_2532109), and glial fibrillary acidic protein (GFAP; an astrocyte marker; 1:250; Abcam, Cat# ab68428, RRID: AB_1209224) overnight at 4°C, followed the next day by incubation with secondary antibodies (1:1000; goat anti-rabbit IgG H&L (Alexa Fluor® 488), Cat# ab150077, RRID: AB_2630356; 1:500; Abcam, goat anti-rabbit IgG H&L (Alexa Fluor® 647), Abcam, Cat# ab150079, RRID: AB_2722623) for 1 hour at room temperature. Images were acquired under a CLSM (LSM 880, Zeiss).

Establishment of rat TBI model and scaffold implantation

A total of 120 male SD rats (12 weeks old, 200–220 g, specific-pathogen-free; Chengdu Dossy) were maintained at 24 ± 2°C, 40% humidity, in a 12-hour light-dark cycling environment, with free access to water and food, and one rat per cage. The rats were divided into four groups using the "random numbers" in QuickCalcs (GraphPad, San Diego, CA, USA): sham group (surgery without TBI, *n* = 30), TBI group (TBI alone, *n* = 30), 3D-CC-NExos group (3D-CC-NExos implantation after TBI, n = 30), and 3D-CC-INExos group (3D-CC-INExos implantation after TBI, *n* = 30). Rats were anesthetized by intraperitoneal injection of 1% pentobarbital sodium (40 mg/kg; MilliporeSigma). Briefly, a 5 mm diameter craniotomy (3.6 mm posterior to the bregma and 2.5 mm to the right of the midline, based on the Rat Brain Atlas; Paxinos and Watson, 2006) was performed to expose the intact dura, as described previously (Liu et al., 2020). The rats were then moved to a stereotaxic frame (RIWARD, Shenzhen, Guangdong, China) and the mold was applied to the brains of rats in the 3D-CC-NExos and 3D-CC-INExos groups to create a lesion cavity 2 mm in diameter and 2 mm in height in the right posterior part of the brain. After sufficient hemostasis, 3D-CC-NExos and 3D-CC-INExos (2 mm in diameter, 2 mm in height) scaffolds were grafted into the cavity, respectively. During this process, the rats' breathing was maintained using a small animal ventilator (RIWARD). Rats in the sham group received a 5 mm diameter craniotomy under anesthesia.

Assessment of functional recovery

Hippocampal-dependent memory and spatial learning from postoperative days 21–28 were assessed using the Morris water maze test (Zhang et al., 2021a, b). The rats' swimming trajectories were captured by making the water opaque using nontoxic ink. The water temperature was adjusted to 22–25°C. The spatial-learning phase was on days 21–26 after TBI. Rats were placed in the pool and trained to find the platform. If the rat found the platform, it was allowed to stay there for 2 seconds, and if the rat failed to find the platform within 60 seconds, it was allowed to ride on the platform for 20 seconds. The time between the rats being placed in the water and finding the platform was identified as the escape latency. The spatial-memory phase was on day 28 after TBI. After the platform was removed, the number of site crossings and the percentage of time spent in the target zone were recorded. Neurological functional recovery was assessed at 1, 3, 7, 14, 21, and 28 days after TBI using modified neurological severity scores (Zhang et al., 2021a, b), consisting of motor tests (tail-lifting test, abnormal activity), sensory tests (vision, touch, proprioception), balance beam test, reflex activity, and abnormal movement. The score ranged from 0–18 points, with 0 being normal and 18 indicating the maximum neurological deficit.

Evaluation of nerve regeneration and repair by histology and TEM

To investigate the nerve regeneration and repair following implantation of 3D-CC-INExos scaffolds, rats were anesthetized by intraperitoneal injection of 1% sodium pentobarbital (40 mg/kg, MilliporeSigma) and then perfused with saline (Chengdu Qingshan Likang Pharmaceutical Co., Ltd., Chengdu, Sichuan, China) 2 months after TBI. Brain tissue was removed, paraffin-embedded, and cut into 5 μm thick slices using an automatic paraffin slice system (MEDITE, Hanover, Germany), as described previously (Jiang et al., 2020b; Zhang et al., 2021b; Liu et al., 2022). To evaluate the damage-repair effects, we compared the general appearance of the damaged area in the model and new tissue in the damaged area by HE staining (Servicebio), Bielschowsky's silver staining (Servicebio), and Nissl staining (Servicebio) 2 months after TBI. For IF, tissue slices were placed in a repair box with EDTA antigen repair buffer (pH 8.0) in a microwave oven for antigen repair. After drying, sections were blocked with 3% bovine serum albumin (Cat# G5001, Servicebio) for 30 minutes and then incubated with the corresponding primary antibodies: rabbit anti-nestin monoclonal antibody (NSC marker; 1:100; Abcam, Cat# ab105389, RRID: AB_10859398); monoclonal rabbit anti-NF antibody (neurofilament marker; 1:500; Abcam, Cat# ab223343, RRID: AB_2891198); monoclonal mouse anti-myelin basic protein (MBP; myelin sheath marker; 1:10; Abcam, Cat# ab11159, RRID: AB_297797); monoclonal rabbit anti-NeuN (neuron marker; 1:1000; Abcam, Cat# ab177487, RRID: AB_2532109); monoclonal rabbit anti-microtubule-associated protein 2 (MAP2; microtubule marker; 1:100; Abcam, Cat# ab183830, RRID: AB_2895301); monoclonal mouse anti-synaptophysin (SYP; synapse marker; 1:50; Abcam, Cat# ab8049, RRID: AB_2198854); monoclonal rabbit anti-CD31 (vascular endothelium marker; 1:1000; Abcam, Cat# ab76533, RRID: AB_1523298); monoclonal mouse anti-α-SMA (vascular smooth muscle marker; 1:500; Abcam, Cat# ab7817, RRID: AB_262054); polyclonal rabbit anti-CD68 (activated macrophage/microglia marker; 1:100; Abcam, Cat# ab125047, RRID: AB_10971844); and monoclonal mouse anti-Iba1 (microglia marker; 1:100; Abcam, Cat# ab283319) at 4°C overnight. The corresponding secondary antibodies were then added: goat anti-rabbit IgG H&L (Alexa Fluor® 488) (1:1000; Abcam, Cat# ab150077, RRID: AB_2630356) and goat anti-rabbit IgG H&L (Alexa Fluor® 647) (1:500; Abcam, Cat# ab150079, RRID: AB_2722623) and donkey anti-mouse IgG H&L (Alexa Fluor® 647) (1:300; Abcam, Cat# ab150107, RRID: AB_2890037) and incubated for 1 hour at 37°C. Samples were incubated with 4′,6-diamidino-2-phenylindole (Bioss, Beijing, China, Cat# S0001) for 8 minutes at room temperature prior to photographing. Apoptosis was detected in TBI-injured areas using a terminal deoxynucleotidyl transferase dUTP nick end labeling (TUNEL) assay kit (Servicebio), according to the manufacturer's instructions (Zhang et al., 2021b). The histological and IF results were quantified by analyzing images at 400 × magnification using ImageJ software (version 7.4; National Institutes of Health, Bethesda, MD, USA). For TEM, brain tissue was removed 2 months after TBI and cut into small pieces (1 mm × 1 mm × 1 mm), fixed in glutaraldehyde for 2 days, and treated sequentially with osmic acid (Ted Pella Inc., Redding, CA, USA), dehydrated, permeated, embedded, and cut into ultrathin sections using an ultrathin slicer (Leica UC7, Leica). After co-staining with uranyl acetate (Hubei Chushengwei Chemical Industry Co. Ltd., Wuhan, Hubei, China) and lead citrate (Shanghai Macklin Biochemical Co., Ltd, Shanghai, China), the samples were photographed by TEM (HT7700, Hitachi) to visualize neurons and myelin sheaths in the injured area after TBI.

***In vivo* safety assessment of scaffolds**

To verify their compatibility *in vivo*, the scaffolds were implanted into the TBI injury cavity of rats and the histomorphology of the heart, lung, liver, spleen, and kidney were assessed at 1 and 2 months after TBI by HE staining (Servicebio). Plasma alanine transaminase, aspartate aminotransferase, blood urea nitrogen, and creatinine were determined by blood biochemistry tests at 1 and 3 days after TBI.

Statistical analysis

The experimenter was blinded to the groups and serial numbers of the animals during the experiments and statistical analysis, and the analysis and experimental groups were assigned by another person. We did not use statistical methods to pre-estimate the sample size, but the sample size was determined with reference to a previous study (Liu et al., 2020). Data are presented as mean ± standard deviation. Groups were compared using two-sample *t*-tests or one-way analyses of variance followed by Student-Newman-Keuls tests. The data were analyzed using SPSS 18.0 statistical software (SPSS, Chicago, IL, USA) and $P < 0.05$ was considered to indicate statistical significance.

Results

Isolation and identification of NSCs from rats

NSCs were isolated from E14 rat brains. There were no differences in the morphology of NSCs with or without IGF-1 pretreatment under light microscopy (**Figure 1A**), and the NSC marker nestin was expressed in cultured NSCs with/without IGF-1 pretreatment in IF experiments (**Figure 1B**).

Characteristics of exosomes from NSCs after IGF-1 pre-stimulation

To confirm the effect of INExos on TBI, exosomes in supernatant from NSCs with or without IGF-1 pre-stimulation were obtained by ultracentrifugation and were confirmed by TEM, NTA, and WB analyses. TEM showed homogeneous, spherical, and membrane vesicles of NExos and INExos (**Figure 1C**). NTA indicated a size distribution of 50–200 nm, with average diameters of 144.3 nm for NExos and 138.9 nm for INExos (**Figure 1D**). Exosomal surface markers, including CD9 and CD63, were expressed in NExos and INExos using WB (**Figure 1E**). Furthermore, there was no difference in exosome concentrations in samples derived from NSCs with or without IGF-1 ($P > 0.05$). These results suggested that NExos and INExos were similar in terms of morphology, particle size, and proteins, indicating that IGF-1 pretreatment had no effect on the exosomal profile of NSCs.

Morphology, microstructure, and properties of 3D-CC-INExos scaffolds

The morphological characteristics of the 3D-printed scaffolds were observed by HE staining, scanning electron microscopy, and CLSM (**Figure 2A–F**). The morphology was homogeneous according to HE staining (**Figure 2B**). Scanning electron microscopy showed that the surfaces of the 3D-printed scaffolds were rough and porous (**Figure 2C** and **D**), providing an advantage for cell adhesion. Exosomes adhered efficiently to the scaffolds (**Figure 2E–G**). The scaffold materials are required to have an appropriate degradation rate. We therefore assessed the degradation rates of scaffolds with five different collagen/chitosan mass ratios (16:1, 8:1, 1:1, 1:8, and 1:16) *in vivo* (**Figure 2H**). The 16:1 and 8:1 scaffolds showed fast degradation (2 weeks), indicating that they would be unable support the damaged area during the

repair process, while the 3D scaffolds with mass ratios of 1:8 and 1:16 had not degraded after 8 weeks, which would result in long-term foreign body residue, which is also not conducive to damage repair. However, 3D-printed scaffolds with a mass ratio of 1:1 were degraded after 4 weeks, which indicated a suitable degradation rate for our study, and scaffolds with a mass ratio of 1:1 were therefore chosen for subsequent experiments. The water absorption and porosity ratios of the scaffolds are key features for supporting tissue regeneration. Both these ratios were better for 3D-printed scaffolds than for ordinary scaffolds by freeze-drying technique (**Figure 2I** and **J**). We also analyzed the release profiles of exosomes in CC-INExos and 3D-CC-INExos scaffolds. 3D-CC-INExos scaffolds showed sustained exosome release for up to 14 days, and > 80% of the unobstructed loaded exosomes were released (**Figure 2K**). IF indicated that exosomes released from scaffolds could be phagocytosed by NSCs (**Figure 2L**).

3D-CC-INExos scaffolds exhibit favorable cytocompatibility and promote neural differentiation of NSCs *in vitro*

NSCs cocultured with 3D-CC-INExos scaffolds showed better cell adhesion than NSCs cocultured with 3D-CC-NExos scaffolds after coculture for 12 hours ($P < 0.05$; **Figure 3A**), and the proliferative capacity of NSCs cocultured with 3D-CC-INExos scaffolds was stronger than that of NSCs cocultured with 3D-CC-INExos scaffolds after 3 days of coculture ($P < 0.05$; **Figure 3B**). It is important to maintain the stemness, normal differentiation, and axonal growth of NSCs during the repair process. The fluorescently labelled phalloidin-dye conjugate clearly showed the morphology and distribution of microfilaments in NSCs under CLSM, and the F-actin-positive area was significantly higher in the 3D-CC-INExos compared with the 3D-CC-NExos scaffold group (**Figure 3C**). Furthermore, the NF-, GAP43-, and NeuN-positive areas were significantly larger in the 3D-CC-INExos compared with the 3D-CC-NExos scaffold group (**Figure 3D–F**). However, GFAP, as a marker of astrocyte activation, was significantly decreased in the 3D-CC-INExos group compared with the 3D-CC-NExos group (**Figure 3G**). These results demonstrate that 3D-CC-INExos could facilitate neural differentiation of NSCs while inhibiting astrocyte differentiation compared with 3D-CC-NExos.

Implanting 3D-CC-INExos further promotes recovery from TBI-induced motor and cognitive deficits

To determine how 3D-printed scaffolds affected TBI-induced cognitive function, rats implanted with the different scaffolds were subjected to the Morris water maze test and the escape latency, quadrant-dwell time, and platform crossing were analyzed. Learning ability was detected during the spatial-learning phase from days 21–26 post-surgery (**Figure 4A**). The escape latency became progressively shorter after training in the sham, TBI, 3D-CC-NExos, and 3D-CC-INExos groups (**Figure 4B**). Rats in the three experimental groups spent significantly more time searching for the hidden platform than sham rats ($P < 0.05$). However, the escape latency was markedly shorter in the 3D-CC-INExos group compared with the 3D-CC-NExos ($P < 0.05$) and TBI groups ($P < 0.01$). The number of site crossings and proportion of time in the target zone were greater in rats from the three experimental groups compared with sham rats ($P < 0.05$) (**Figure 4C** and **D**). Rats in the 3D-CC-INExos group showed significant improvements in the number of site crossings and proportion of time in the target zone compared with both the TBI and 3D-CC-NExos groups ($P < 0.05$) (**Figure 4C** and **D**), suggesting that implantation of the 3D-CC-INExos scaffold improved learning and memory abilities. Motor coordination and sensory abilities were assessed using the modified neurological severity scores (**Figure 4E**). The modified neurological severity score in the sham-operated group was almost zero, while rats in the other three groups achieved high scores on the first postoperative day, indicating severe impairment. Compared with the TBI and 3D-CC-NExos groups, rats in the 3D-CC-INExos group showed a more significant downward trend on postoperative day 28 ($P < 0.05$), indicating that implantation of 3D-CC-INExos scaffolds in damaged areas after TBI could significantly improve motor coordination and sensory performance.

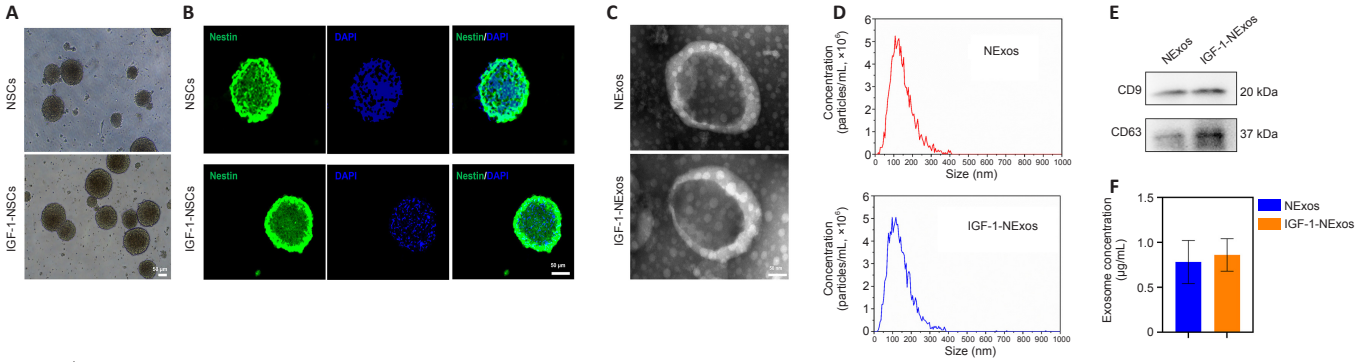

Figure 1 | **Identification of NSCs and characteristics of exosomes from NSCs.**
(A) Morphology of NSCs with or without IGF-1 pretreatment under a light microscope. Scale bar: 50 μm. (B) Immunofluorescence staining images of nestin (green) in NSCs with or without IGF-1 pretreatment. Scale bar: 50 μm. (C) Morphology of exosomal structures observed by transmission electron microscopy. Scale bar: 50 nm. (D) Particle size distribution of exosomes measured by nanoparticle tracking analysis. (E) Exosomal markers detected by western blot analyses. (F) Exosome concentrations of NExos and INExos. DAPI: 4′,6-Diamidino-2-phenylindole; IGF-1: insulin-like growth factor 1; NSCs: neural stem cells. NExos: Exosomes extracted from supernatant of NSCs cultured in ordinary complete medium; IGF-1-NExos (INExos): exosomes extracted from supernatant of NSCs cultured in ordinary complete medium supplemented with IGF-1.

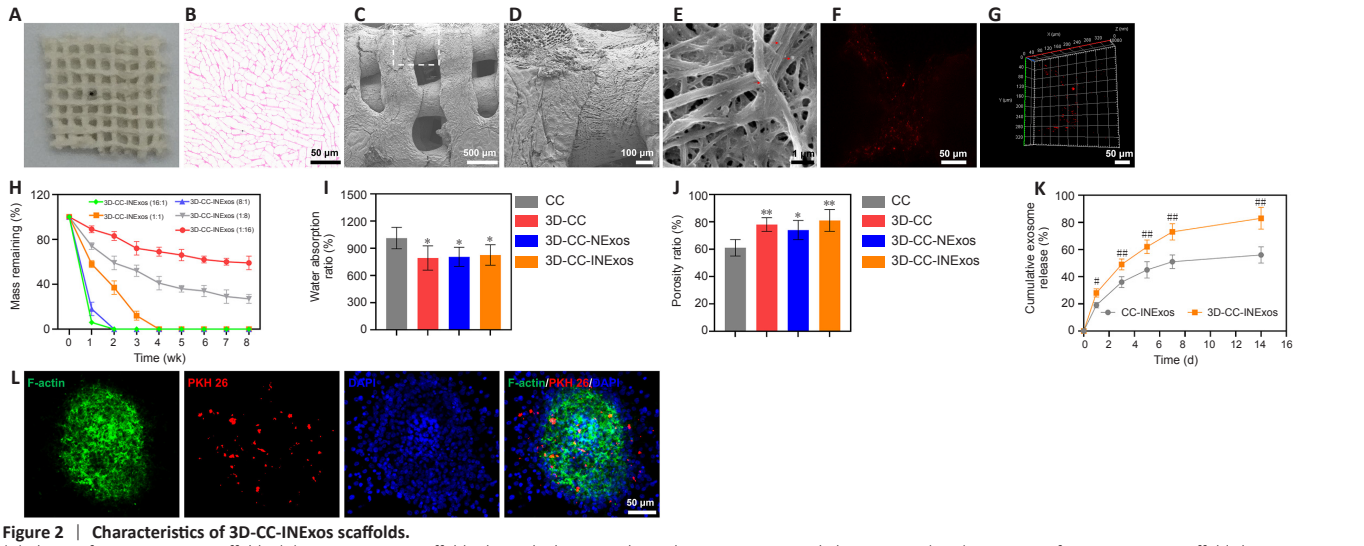

Figure 2 | **Characteristics of 3D-CC-INExos scaffolds.**
(A) Shape of 3D-CC-INExos scaffolds. (B) 3D-CC-INExos scaffolds shown by hematoxylin and eosin staining. Scale bar: 50 μm. (C, D) Structure of 3D-CC-INExos scaffolds by SEM micrographs (D is enlarged image of white box in C). Scale bars: 500 μm in C, 100 μm in D. (E) SEM micrographs showing exosomes (red arrows) adhered to 3D-CC-INExos scaffolds. Scale bar: 1 μm. (F, G) Immunofluorescence staining images revealed distribution of exosomes in scaffolds. Scale bars: 50 μm. (H) Degradation time curves of scaffolds with different ratios. (I, J) Water absorption (I) and porosity ratios (J) of scaffolds. (K) Cumulative release curves of exosomes from scaffolds within 14 days. (L) IF images showing exosomes labeled with PKH26 (red) released from scaffolds phagocytosed by NSCs (F-actin, green). Scale bars: 50 μm. *$P < 0.05$, **$P < 0.01$, *vs.* CC; #$P < 0.05$, ##$P < 0.01$, *vs.* CC-INExos (two-sample *t*-tests or one-way analyses of variance followed by Student-Newman-Keuls tests; experiment repeated five times). Four kinds of scaffolds were used: collagen/chitosan (CC), 3D-printed collagen/chitosan (3D-CC), 3D-printed collagen/chitosan/NExos (3D-CC-NExos), and 3D-printed collagen/chitosan/INExos scaffolds (3D-CC-INExos). NExos: exosomes extracted from supernatant of NSCs cultured in ordinary complete medium; IGF-1-NExos (INExos): exosomes extracted from supernatant of NSCs cultured in ordinary complete medium supplemented with IGF-1. DAPI: 4′,6-Diamidino-2-phenylindole; NSCs: neural stem cells; IGF-1: insulin-like growth factor 1; SEM: scanning electron microscopy.

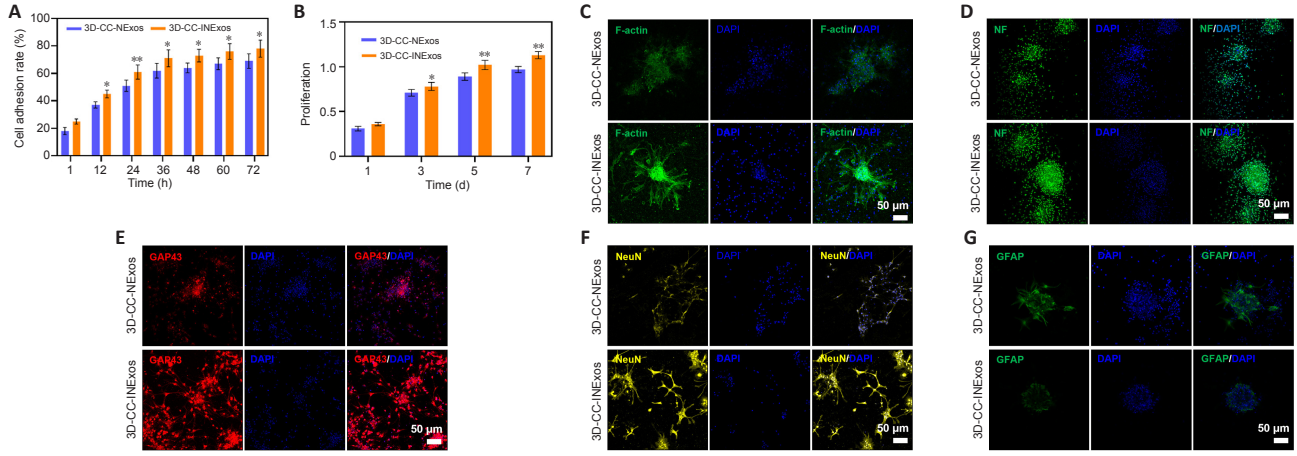

Figure 3 | Good biocompatibility of 3D-CC-INExos scaffolds and effects on neural differentiation of NSCs.
(A) Cell adhesion rate of NSCs cocultured with scaffolds. (B) Proliferative capacity of NSCs cocultured with scaffolds. (C–G) Typical images of F-actin (green) (C), NF (green) (D), GAP43 (red) (E), NeuN (yellow) (F), and GFAP (green) (G) after coculture of NSCs with 3D-CC-NExos and 3D-CC-INExos. Scale bars: 50 μm. Data are presented as mean ± SD. *P < 0.05, **P < 0.01, *vs*. 3D-CC-NExos (two-sample *t*-tests or one-way analyses of variance followed by Student-Newman-Keuls tests; experiments repeated five times). 3D-CC-NExos: 3D-printed collagen/chitosan/NExos; 3D-CC-INExos: 3D-printed collagen/chitosan/INExos scaffolds. NExos: Exosomes extracted from supernatant of NSCs cultured in ordinary complete medium; IGF-1-NExos (INExos): exosomes extracted from supernatant of NSCs cultured in ordinary complete medium supplemented with IGF-1. DAPI: 4′,6-Diamidino-2-phenylindole; GAP43: growth associated protein-43; GFAP: glial fibrillary acidic protein; IGF-1: insulin-like growth factor 1; NeuN: neuronal nuclear protein; NF: neurofilament.

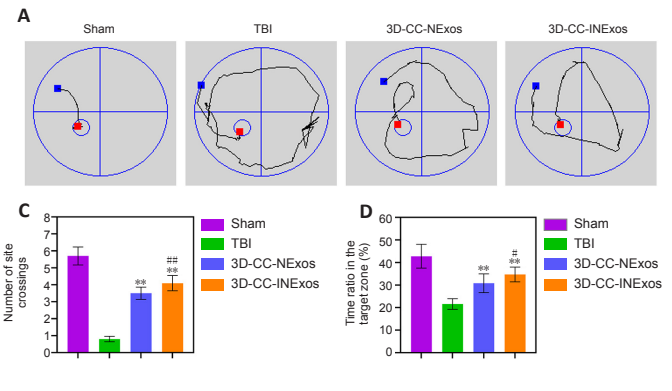

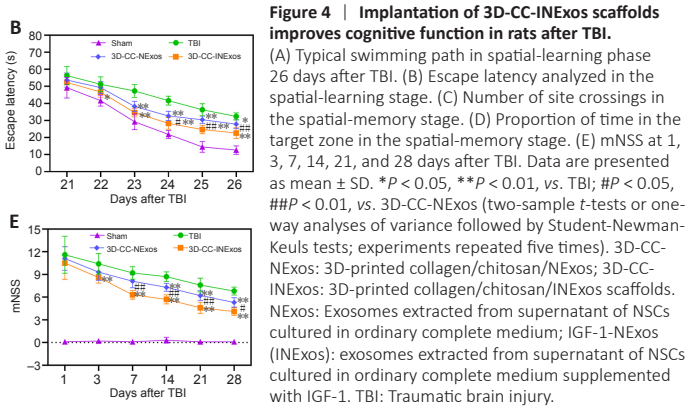

Figure 4 | Implantation of 3D-CC-INExos scaffolds improves cognitive function in rats after TBI.
(A) Typical swimming path in spatial-learning phase 26 days after TBI. (B) Escape latency analyzed in the spatial-learning stage. (C) Number of site crossings in the spatial-memory stage. (D) Proportion of time in the target zone in the spatial-memory stage. (E) mNSS at 1, 3, 7, 14, 21, and 28 days after TBI. Data are presented as mean ± SD. *P < 0.05, **P < 0.01, *vs*. TBI; #P < 0.05, ##P < 0.01, *vs*. 3D-CC-NExos (two-sample *t*-tests or one-way analyses of variance followed by Student-Newman-Keuls tests; experiments repeated five times). 3D-CC-NExos: 3D-printed collagen/chitosan/NExos; 3D-CC-INExos: 3D-printed collagen/chitosan/INExos scaffolds. NExos: Exosomes extracted from supernatant of NSCs cultured in ordinary complete medium; IGF-1-NExos (INExos): exosomes extracted from supernatant of NSCs cultured in ordinary complete medium supplemented with IGF-1. TBI: Traumatic brain injury.

Implanting 3D-CC-INExos improves brain tissue regeneration and nerve repair in damaged areas

To assess the reparative effects of the scaffolds in the damaged area, we compared the general appearance of the damaged area in the model and the development of new tissue 2 months after TBI by HE, silver, and Nissl staining. There was no loss of brain tissue and no obvious changes in cell morphology in the sham group. However, the damaged tissue was obviously repaired better in the 3D-CC-INExos group compared with the other two experimental groups, based on the general appearance (**Figure 5A**). Rats in the TBI group showed massive tissue loss evident from the general appearance, and HE staining showed few regenerated cells (**Figure 5B** and **C**). In contrast, rats in the 3D-CC-NExos and 3D-CC-INExos groups showed obvious brain tissue regeneration in terms of overall appearance, and HE staining showed regenerated cells in the injured area in the 3D-CC-INExos group. The regenerative effect of 3D-CC-INExos was better than that of 3D-CC-NExos for TBI. The extent of Bielschowsky's silver staining was significantly wider in the 3D-CC-INExos and 3D-CC-NExos groups than in the TBI group (P < 0.01; **Figure 5D** and **E**). These results indicated that the 3D-printed scaffolds improved brain tissue repair. In addition, the number of nerve fibers in the injured area was significantly greater in the 3D-CC-INExos group than in the 3D-CC-NExos group (P < 0.01). Similarly, Nissl bodies, as neuronal markers, were denser and more widely distributed in the injured area in the 3D-CC-INExos group (P < 0.01; **Figure 5F** and **G**). These results demonstrated that implantation of the 3D-CC-INExos scaffold had a better effect than the 3D-CC-NExos scaffold on the regeneration of nerve fibers and neurons after TBI.

Implanting 3D-CC-INExos increases recruitment of endogenous NSCs and improves nerve tissue regeneration after TBI

We investigated nerve regeneration of TBI after treatment with 3D-CC-INExos using IF and TEM. IF using an antibody against the NSC marker nestin revealed significantly more NSCs in the damaged area in the 3D-CC-INExos group (P < 0.01; **Figure 6A** and **B**), indicating that 3D-CC-INExos scaffolds could recruit NSCs to the injured area after TBI. IF was also carried out using NF, MBP, and NeuN antibodies to assess the regeneration of nerve fibers, myelin sheaths, and mature neurons in the injured area at 2 months post-injury, respectively (**Figure 7A**). Implantation of the 3D-CC-INExos scaffold in the injured area increased the numbers of nerve fibers, myelin sheaths, and mature neurons compared with the 3D-CC-NExos scaffold (P < 0.05; **Figure 7B–D**). We further assessed the effect of the scaffolds on synapse formation by dual IF labelling with specific markers (MAP2 and SYP). MAP2- and SYP-positive cells were significantly increased in the 3D-CC-INExos compared with the TBI and 3D-CC-NExos groups (**Figure 7E–G**). In conclusion, these results demonstrate that implantation of a 3D-CC-INExos scaffold could enhance neural regeneration after TBI. Finally, we observed the neuronal structures, number of axons, and diameter and thickness of the myelin sheath in the injured area 2 months after TBI using TEM (**Figure 7H**), which showed that implantation of the 3D-CC-INExos scaffold not only ameliorated neuronal structures but also increased the diameter and thickness of the myelin sheath.

3D-CC-INExos scaffold improves angiogenesis and inhibits inflammation and apoptosis in the injured area after TBI

We evaluated the effects of the scaffolds on angiogenesis, inflammation, and apoptosis in the injured area 2 months after TBI by IF and TUNEL staining. More cells expressing CD31 and α-SMA (specific markers of angiogenesis) were found in the injured area of 3D-CC-INExos compared with TBI and 3D-CC-NExos (**Figure 8A**). These data suggest that implanting 3D-CC-INExos could improve angiogenesis. In addition, expression of CD68 and Iba-1 in the lesion area was decreased in the 3D-CC-INExos group (**Figure 8B**), indicating that 3D-CC-INExos treatment further suppressed inflammation, and fewer TUNEL-positive signals were captured in the 3D-CC-INExos scaffold group (**Figure 8C**). These results suggest that 3D-CC-INExos scaffolds could further enhance angiogenesis while suppressing inflammation and inhibiting cell apoptosis in the lesion area.

Histocompatibility of scaffolds *in vivo*

Exosomes have demonstrated excellent biocompatibility; however, we further examined the tolerance to the scaffolds *in vivo*. The scaffolds were implanted into the TBI injury cavity of rats. HE staining showed no pathological abnormalities in the heart, lung, liver, spleen, or kidney in the TBI, 3D-CC-NExos, and 3D-CC-INExos groups compared with the sham group (**Figure 9A**). Hematological analysis also showed no significant differences in liver and kidney functional indicators in the scaffold groups compared with the sham group (**Figure 9B**). These results suggested that the scaffolds were biocompatible *in vivo*.

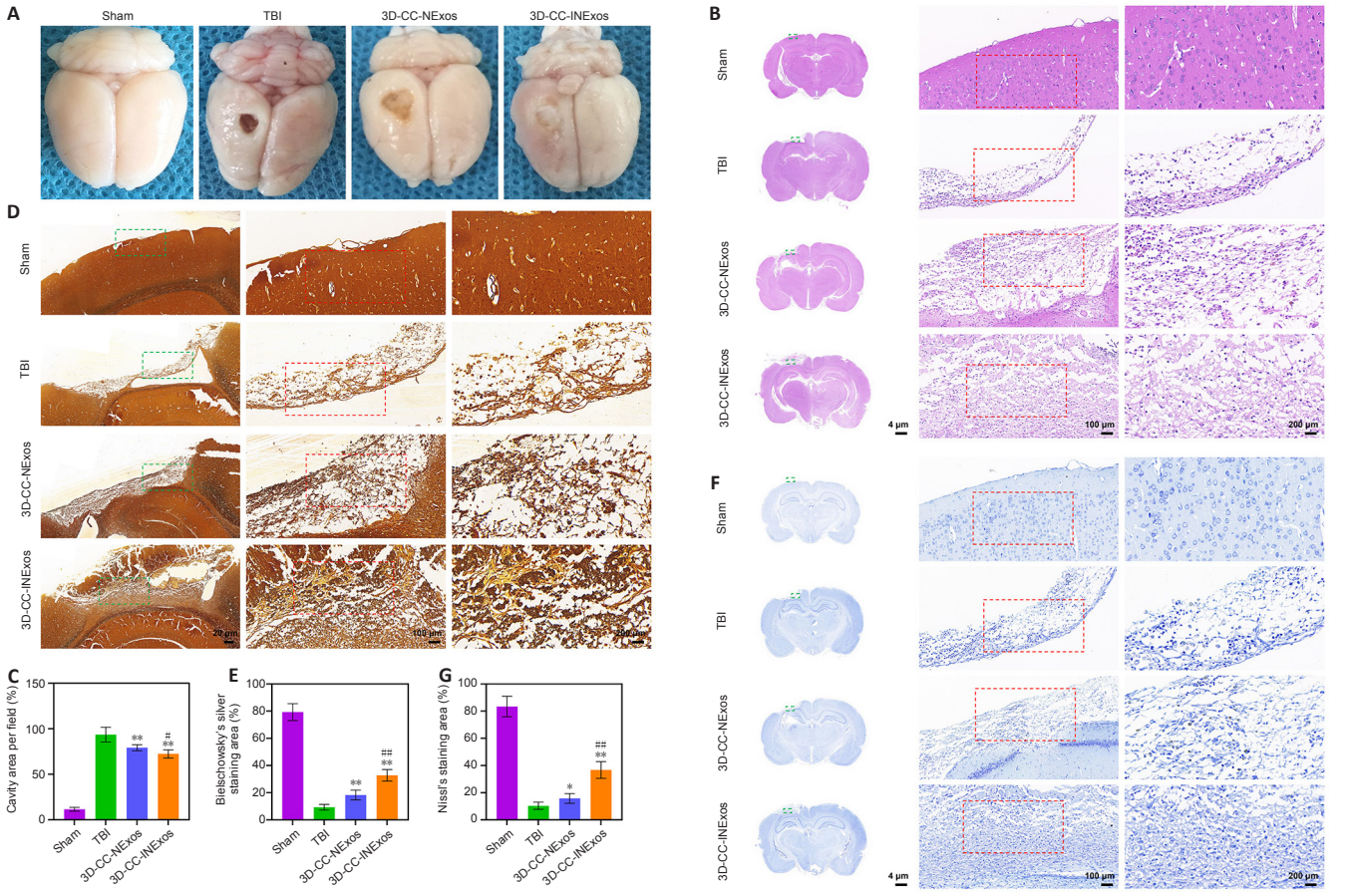

Figure 5 | **Tissue regeneration and reparative ability of scaffolds *in vivo* 2 months after TBI.**
(A) General images of damaged area in the TBI model. (B) Representative hematoxylin and eosin (HE) staining images of damaged area in sham, TBI, 3D-CC-NExos, and 3D-CC-INExos groups. Middle image is enlarged image of green box in left-hand image; right-hand image is enlarged image of red box in middle image. (C) Quantitative statistical analysis of HE staining. (D) Representative Bielschowsky's silver staining images of damaged area in sham, TBI, 3D-CC-NExos, and 3D-CC-INExos groups. Middle image is enlarged image of green box in left-hand image; right-hand image is enlarged image of red box in middle image. (E) Quantitative statistical analysis of Bielschowsky's silver staining. (F) Representative Nissl staining images of damaged area in sham, TBI, 3D-CC-NExos, and 3D-CC-INExos groups. (G) Quantitative statistical analysis of Nissl staining. Middle image is enlarged image of green box in left-hand image; right-hand image is enlarged image of red box in middle image. Data are presented as mean ± SD. *P < 0.05, **P < 0.01, *vs.* TBI; #P < 0.05, ##P < 0.01, *vs.* 3D-CC-NExos (two-sample t-tests or one-way analyses of variance followed by Student-Newman-Keuls tests; experiments repeated five times). 3D-CC-NExos: 3D-printed collagen/chitosan/NExos; 3D-CC-INExos: 3D-printed collagen/chitosan/INExos scaffolds. NExos: Exosomes extracted from supernatant of NSCs cultured in ordinary complete medium; IGF-1-NExos (INExos): exosomes extracted from supernatant of NSCs cultured in ordinary complete medium supplemented with IGF-1. TBI: traumatic brain injury.

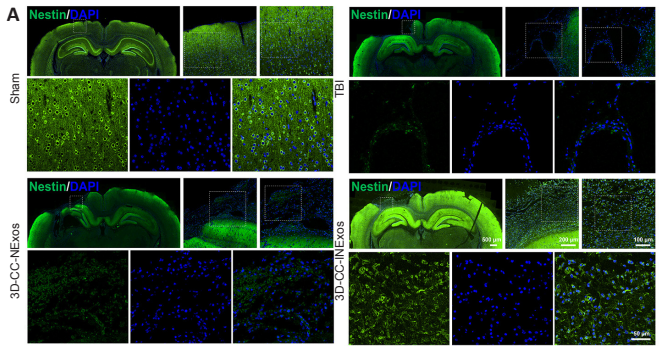

Figure 6 | **IF analysis of NSC recruitment in damaged area 2 months post-injury.**
(A) Typical IF images of nestin (green) in the lesion area in sham, TBI, 3D-CC-NExos, and 3D-CC-INExos groups. Middle image is enlarged image of white box in left-hand image; right-hand image is enlarged image of white box in middle image; image below is enlarged image of white box in right-hand image. (B) Quantitative analysis of nestin-positive cells in lesion area in each group. Data are presented as mean ± SD. **P < 0.01 *vs.* TBI; ##P < 0.01 *vs.* 3D-CC-NExos (two-sample *t*-tests or one-way analyses of variance followed by Student-Newman-Keuls tests; experiments repeated five times). 3D-CC-NExos: 3D-printed collagen/chitosan/NExos; 3D-CC-INExos: 3D-printed collagen/chitosan/INExos scaffolds. NExos: Exosomes extracted from supernatant of NSCs cultured in ordinary complete medium; IGF-1-NExos (INExos): exosomes extracted from supernatant of NSCs cultured in ordinary complete medium supplemented with IGF-1. IF: Immunofluorescence staining; TBI: traumatic brain injury.

Discussion

In this study, we investigated the use of 3D-printed collagen/chitosan scaffolds loaded with exosomes derived from NSCs pretreated with IGF-1 (3D-CC-INExos) to bridge injured areas and improve functional recovery after TBI in SD rats. We evaluated the effect of scaffold transplantation 2 months post-injury. We first assessed the tissue-regenerative effects of the 3D-CC-INExos scaffolds using HE, Bielschowsky's silver, and Nissl staining, IF, and TEM, and then evaluated the effect of scaffold transplantation on the functional recovery of rats after TBI. Finally, we assessed the local effects and systemic histocompatibility of the scaffolds. The results indicated that 3D-CC-INExos implantation promoted the recovery of motor and cognitive deficits, improved brain tissue regeneration and nerve repair, increased angiogenesis, and reduced local inflammation and cell apoptosis in the injured area after TBI, suggesting that implanting 3D-CC-INExos scaffolds may be a suitable treatment for TBI. As an experimental study, these results successfully validated the effectiveness of 3D-CC-INExos for TBI repair by examining the actual therapeutic effects, such as the restoration of neurological, behavioral, and cognitive functions. Coupling collagen with chitosan can inhibit the rapid degradation of collagen and ameliorate its mechanical strength, and enhance the biocompatibility of chitosan, suggesting that this combination is a reliable carrier for low-temperature 3D-printed scaffolds (Suo et al., 2021).

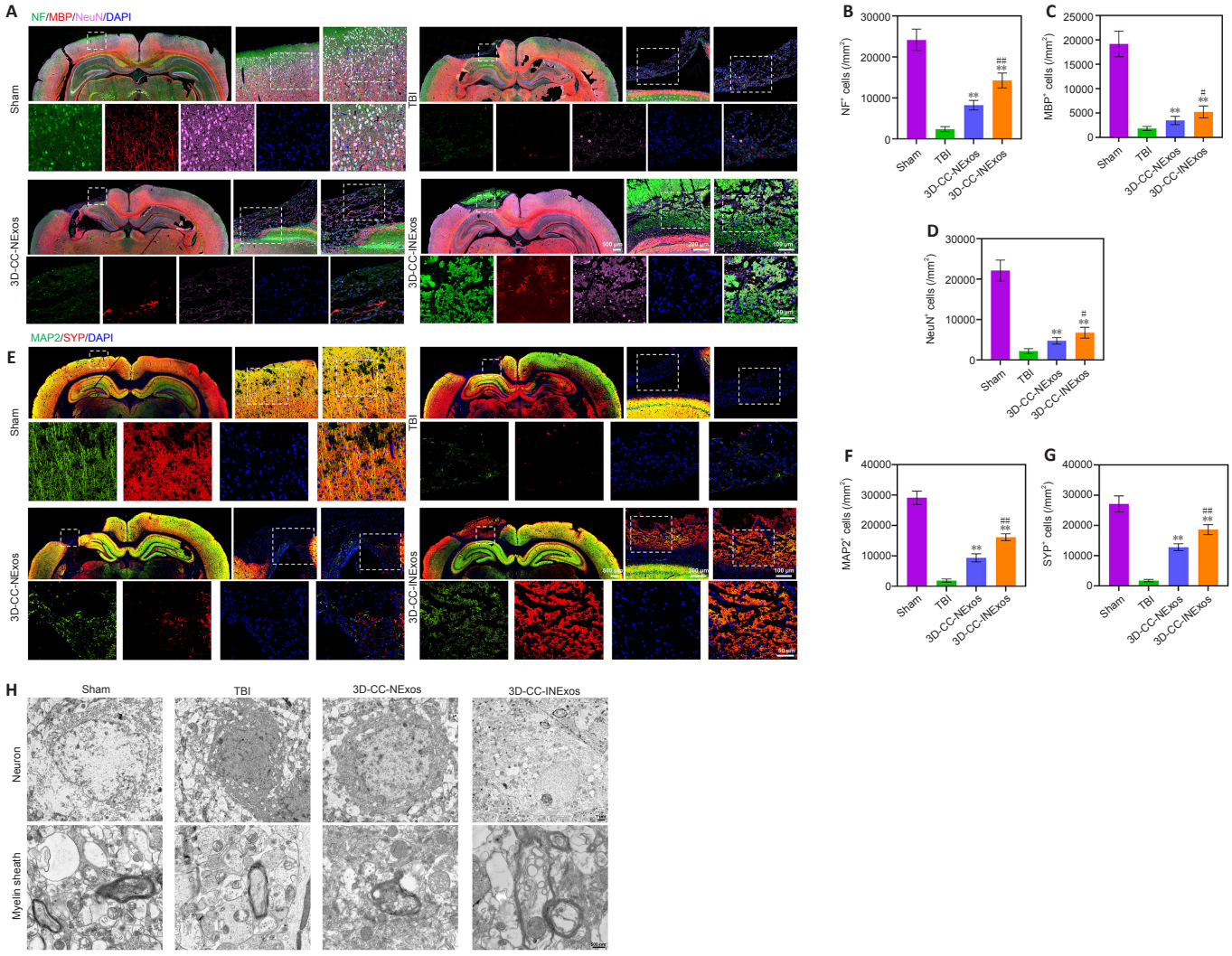

Figure 7 | **Regeneration of nerve fibers, myelin sheaths, and axons 2 months post-injury.**
(A) Typical IF images of NF (green), MBP (red), and NeuN (pink) in lesion area in sham, TBI, 3D-CC-NExos, and 3D-CC-INExos groups. Middle image is enlarged image of white box in left-hand image; right-hand image is enlarged image of white box in middle image; image below is enlarged image of white box in right-hand image. (B–D) Quantification of NF- (B), MBP- (C), and NeuN- (D) positive cells in lesion area in each group. (E) Typical IF images of MAP2 (green) and SYP (red) in lesion area in sham, TBI, 3D-CC-NExos, and 3D-CC-INExos groups. Middle image is enlarged image of white box in left-hand image; right-hand image is enlarged image of white box in middle image; image below is enlarged image of white box in right-hand image. (F–G) Quantification of MAP2- (F) and SYP-positive (G) cells in lesion area in each group. (H) Typical TEM images of lesion area in each group. Scale bars: 500 nm in H. Data are presented as mean ± SD. $^{**}P < 0.01$, *vs.* TBI; $^{\#}P < 0.05$, $^{\#\#}P < 0.01$, *vs.* 3D-CC-NExos (two-sample *t*-tests or one-way analyses of variance followed by Student-Newman-Keuls tests; experiments repeated five times). 3D-CC-NExos: 3D-printed collagen/chitosan/NExos; 3D-CC-INExos: 3D-printed collagen/chitosan/INExos scaffolds. NExos: Exosomes extracted from supernatant of NSCs cultured in ordinary complete medium; IGF-1-NExos (INExos): exosomes extracted from supernatant of NSCs cultured in ordinary complete medium supplemented with IGF-1. DAPI: 4′,6-Diamidino-2-phenylindole; IF: Immunofluorescence staining; MAP2: microtubule-associated protein 2; MBP: myelin basic protein; NeuN: neuronal nuclear protein; NF: neurofilament; SYP: synaptophysin; TBI: traumatic brain injury.

Collagen/chitosan scaffolds combined with IGF-1-pretreated NSC-exosomes under low-temperature 3D-printing not only ensured exosome activity, but also enabled the continuous release and detection of exosomes from the 3D-CC-INExos scaffolds for up to 14 days *in vitro*. Exosomes have diverse compositions, including proteins, miRNAs, and mRNAs, giving them unique properties that mediate cell-to-cell communication and interactions, and they play a significant role in the regeneration of NSCs (Zhang et al., 2021c; Kimiz-Gebologlu and Oncel, 2022). The growth hormone-IGF-1 system plays a key role in regulating adult neurogenesis, brain plasticity, and cell survival (Szarka et al., 2021), with a direct or mediated effect through its downstream hormone IGF-1 (Tenuta et al., 2021). Furthermore, high serum IGF-1 levels were shown to improve white matter and memory recovery after TBI (Feeney et al., 2017). IGF-1 modulated adult neurogenesis, brain plasticity, and cell survival (LLorens-Martin et al., 2009) and improved white matter recovery and memory improvement after TBI, but the mechanism remains unclear (Bianchi et al., 2017). The current results demonstrated that the effect of IGF-1 on neural regeneration after TBI is mediated in part by stimulating the release of exosomes from NSCs.

This study had several limitations. First, this was an animal study conducted in rats, and the body structure and function of rats differ from those of humans. In addition, the mechanisms of the 3D-CC-INExos scaffold in NSC proliferation, migration, and differentiation have not been elucidated, and the mechanisms underlying its effects on neural regeneration and neuroprotection have also not been revealed.

In conclusion, implanting 3D-CC-INExos scaffolds could increase the recruitment of endogenous NSCs, improve neural regeneration, ameliorate angiogenesis, and inhibit inflammation and apoptosis, thus improving neurological functional recovery after TBI.

Author contributions: *Study design: XYL, YHF, QBF, YRH, XYC, LXZ; experiment implementation and manuscript drafting: XYL, YHF, QBF, JYZ, LZ, PL, SW; manuscript revising and modifying: XYL, YHF, QBF, YRH, XYC, LXZ, JYZ, LZ; table and figure preparation: XYL, YHF, QBF, JYZ, LZ, PL, SW; manuscript proposing and editing: XYL, YHF, QBF, YRH, XYC, LXZ. All authors read and approved the final manuscript.*
Conflicts of interest: *There are no actual or potential conflicts of interest.*
Data availability statement: *No additional data are available.*

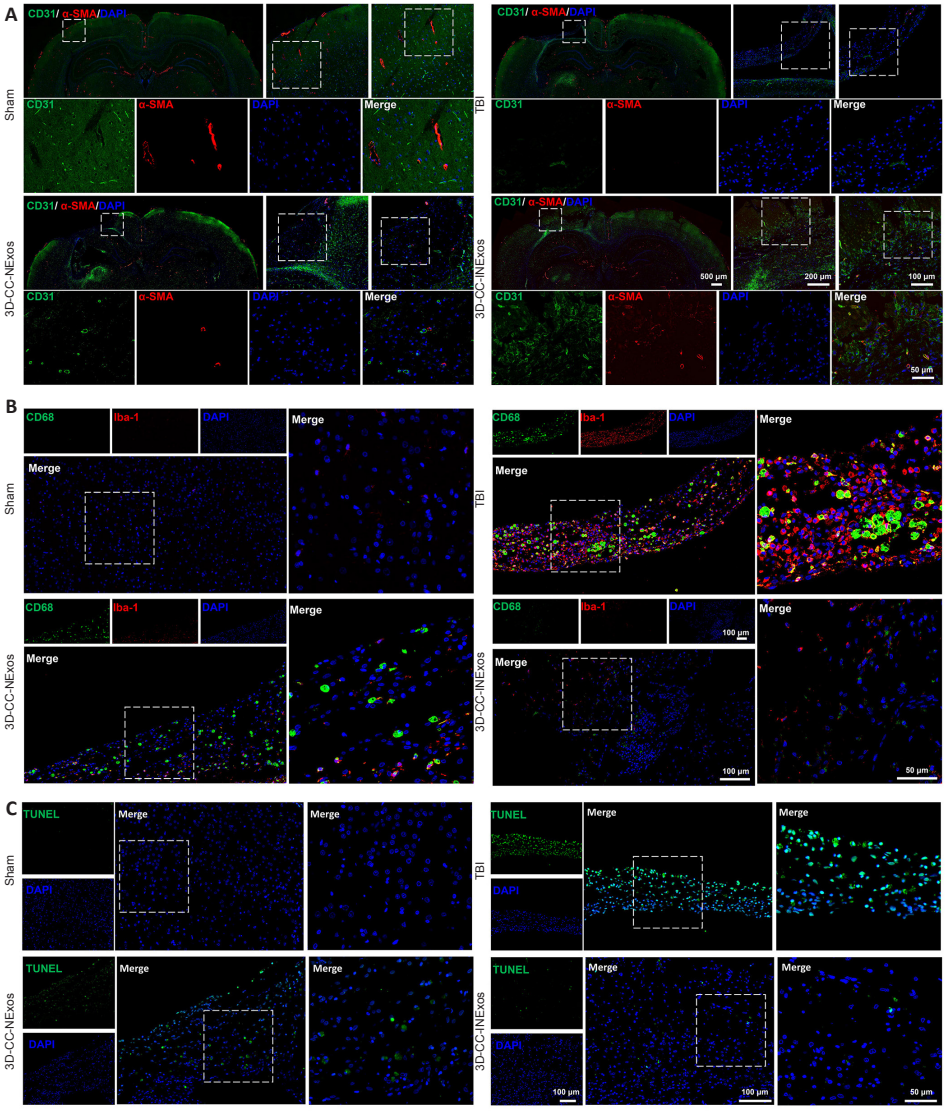

Figure 8 | Angiogenesis, inflammation, and apoptosis in the injured area 2 months post-injury.
(A) Typical IF images of angiogenesis markers CD31 (green) and α-SMA (red) in lesion area in sham, TBI, 3D-CC-NExos, and 3D-CC-INExos groups. Middle image is enlarged image of white box in left-hand image; right-hand image is enlarged image of white box in middle image; image below is enlarged image of white box in right-hand image. (B) Typical immunofluorescence staining images of inflammatory markers CD68 (green) and Iba-1 (red) in lesion area in sham, TBI, 3D-CC-NExos, and 3D-CC-INExos groups. Right-hand image is enlarged image of white box in left-hand image. (C) Typical images of TUNEL staining (green) for apoptosis in lesion area in sham, TBI, 3D-CC-NExos, and 3D-CC-INExos groups. Right-hand image is enlarged image of white box in left-hand image. 3D-CC-NExos: 3D-printed collagen/chitosan/NExos; 3D-CC-INExos: 3D-printed collagen/chitosan/INExos scaffolds. NExos: Exosomes extracted from supernatant of NSCs cultured in ordinary complete medium; IGF-1-NExos (INExos): exosomes extracted from supernatant of NSCs cultured in ordinary complete medium supplemented with IGF-1. α-SMA: Alpha smooth muscle actin; Iba1: ionized calcium binding adaptor molecule 1; TUNEL: terminal deoxynucleotidyl transferase dUTP nick-end labeling; DAPI: 4′,6-diamidino-2-phenylindole.

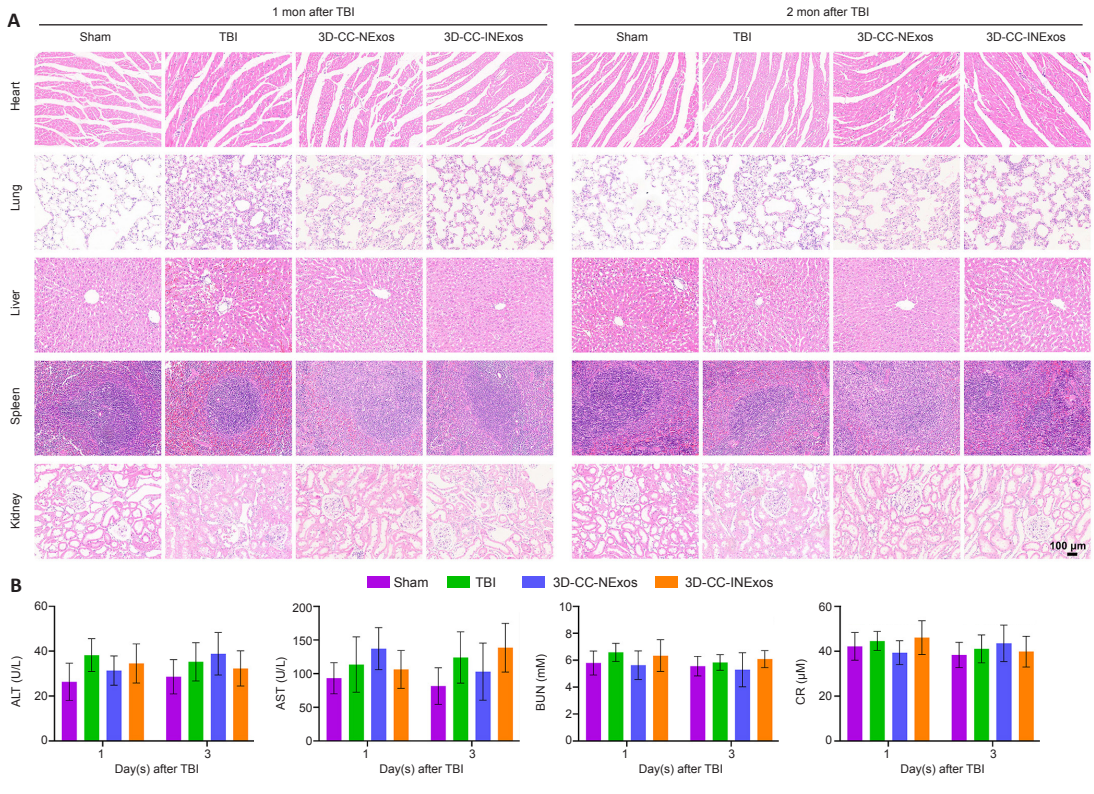

Figure 9 | Biocompatibility of scaffolds *in vivo*.
(A) Representative HE staining of the heart, lung, liver, spleen, and kidney in sham, TBI, 3D-CC-NExos, and 3D-CC-INExos groups 1 month after TBI and 2 months post-injury. Scale bar: 100 μm. (B) ALT, AST, BUN, and CR levels. Data are presented as mean ± SD. Experiments repeated five times. 3D-CC-NExos: 3D-printed collagen/chitosan/NExos; 3D-CC-INExos: 3D-printed collagen/chitosan/INExos scaffolds. NExos: Exosomes extracted from supernatant of NSCs cultured in ordinary complete medium; IGF-1-NExos (INExos): exosomes extracted from supernatant of NSCs cultured in ordinary complete medium supplemented with IGF-1. ALT: Alanine transaminase; AST: aspartate aminotransferase; BUN: blood urea nitrogen; CR: creatinine.

References

Acosta SA, Tajiri N, Hoover J, Kaneko Y, Borlongan CV (2015) Intravenous bone marrow stem cell grafts preferentially migrate to spleen and abrogate chronic inflammation in stroke. Stroke 46:2616-2627.

Ayer-le Lievre C, Stahlbom PA, Sara VR (1991) Expression of IGF-I and-II mRNA in the brain and craniofacial region of the rat fetus. Development 111:105-115.

Bianchi VE, Locatelli V, Rizzi L (2017) Neurotrophic and neuroregenerative effects of GH/IGF1. Int J Mol Sci 18:2441.

Chen Y, Lin J, Yan W (2022) A prosperous application of hydrogels with extracellular vesicles release for traumatic brain injury. Front Neurol 13:908468.

Cui L, Saeed Y, Li H, Yang J (2022) Regenerative medicine and traumatic brain injury: from stem cell to cell-free therapeutic strategies. Regen Med 17:37-53.

Dooley D, Vidal P, Hendrix S (2014) Immunopharmacological intervention for successful neural stem cell therapy: New perspectives in CNS neurogenesis and repair. Pharmacol Ther 141:21-31.

Feeney C, Sharp DJ, Hellyer PJ, Jolly AE, Cole JH, Scott G, Baxter D, Jilka S, Ross E, Ham TE, Jenkins PO, Li LM, Gorgoraptis N, Midwinter M, Goldstone AP (2017) Serum insulin-like growth factor-I levels are associated with improved white matter recovery after traumatic brain injury. Ann Neurol 82:30-43.

Gao G, Wu X, Feng J, Hui J, Mao Q, Lecky F, Lingsma H, Maas AIR, Jiang J, China C-TBIRP (2020) Clinical characteristics and outcomes in patients with traumatic brain injury in China: a prospective, multicentre, longitudinal, observational study. Lancet Neurol 19:670-677.

Garbuzova-Davis S, Kurien C, Thomson A, Falco D, Ahmad S, Staffetti J, Steiner G, Abraham S, James G, Mahendrasah A, Sanberg PR, Borlongan CV (2017) Endothelial and astrocytic support by human bone marrow stem cell grafts into symptomatic ALS mice towards blood-spinal cord barrier repair. Sci Rep 7:884.

Goldman SA (2016) Stem and Progenitor cell-based therapy of the central nervous system: hopes, hype, and wishful thinking. Cell Stem Cell 18:174-188.

Gonzalez R, Garitaonandia I, Poustovoitov M, Abramihina T, McEntire C, Culp B, Attwood J, Noskov A, Christiansen-Weber T, Khater M, Mora-Castilla S, To C, Crain A, Sherman G, Semechkin A, Laurent LC, Elsworth JD, Sladek J, Snyder EY, Redmond DE Jr, et al. (2016) Neural stem cells derived from human parthenogenetic stem cells engraft and promote recovery in a nonhuman primate model of Parkinson's disease. Cell Transplant 25:1945-1966.

Hacene S, Le Friec A, Desmoulin F, Robert L, Colitti N, Fitremann J, Loubinoux I, Cirillo C (2022) Present and future avenues of cell-based therapy for brain injury: The enteric nervous system as a potential cell source. Brain Pathol 32:e13105.

Han M, Yang H, Lu X, Li Y, Liu Z, Li F, Shang Z, Wang X, Li X, Li J, Liu H, Xin T (2022) Three-dimensional-cultured MSC-derived exosome-hydrogel hybrid microneedle array patch for spinal cord repair. Nano Lett 22:6391-6401.

Harris J, Lee H, Tu CT, Cribbs D, Cotman C, Jeon NL (2007) Preparing e18 cortical rat neurons for compartmentalization in a microfluidic device. J Vis Exp:305.

Hattiangady B, Shetty AK (2012) Neural stem cell grafting counteracts hippocampal injury-mediated impairments in mood, memory, and neurogenesis. Stem Cells Transl Med 1:696-708.

Hu Y, Tao R, Chen L, Xiong Y, Xue H, Hu L, Yan C, Xie X, Lin Z, Panayi AC, Mi B, Liu G (2021a) Exosomes derived from pioglitazone-pretreated MSCs accelerate diabetic wound healing through enhancing angiogenesis. J Nanobiotechnology 19:150.

Hu YQ, Wu B, Xiong Y, Tao RY, Panayi AC, Chen L, Tian WQ, Xue H, Shi L, Zhang XL, Xiong LM, Mi BB, Liu GH (2021b) Cryogenic 3D printed hydrogel scaffolds loading exosomes accelerate diabetic wound healing. Chem Eng J 10.1016/j.cej.2021.130634.

Iraci N, Gaude E, Leonardi T, Costa ASH, Cossetti C, Peruzzotti-Jametti L, Bernstock JD, Saini HK, Gelati M, Vescovi AL, Bastos C, Faria N, Occhipinti LG, Enright AJ, Frezza C, Pluchino S (2017) Extracellular vesicles are independent metabolic units with asparaginase activity. Nat Chem Biol 13:951-955.

Jiang J, Liu X, Chen H, Dai C, Niu X, Dai L, Chen X, Zhang S (2020a) 3D printing collagen/heparin sulfate scaffolds boost neural network reconstruction and motor function recovery after traumatic brain injury in canine. Biomater Sci 8:6362-6374.

Jiang JP, Liu XY, Zhao F, Zhu X, Li XY, Niu XG, Yao ZT, Dai C, Xu HY, Ma K, Chen XY, Zhang S (2020b) Three-dimensional bioprinting collagen/silk fibroin scaffold combined with neural stem cells promotes nerve regeneration after spinal cord injury. Neural Regen Res 15:959-968.

Jiao Y, Liu YW, Chen WG, Liu J (2022) Neuroregeneration and functional recovery after stroke: advancing neural stem cell therapy toward clinical application. Neural Regen Res 16:80-92.

Kim HY, Kim TJ, Kang L, Kim YJ, Kang MK, Kim J, Ryu JH, Hyeon T, Yoon BW, Ko SB, Kim BS (2020) Mesenchymal stem cell-derived magnetic extracellular nanovesicles for targeting and treatment of ischemic stroke. Biomaterials 243:119942.

Kimiz-Gebologlu I, Oncel SS (2022) Exosomes: Large-scale production, isolation, drug loading efficiency, and biodistribution and uptake. J Control Release 347:533-543.

Liu X, Zhang G, Wei P, Zhong L, Chen Y, Zhang J, Chen X, Zhou L (2022) Three-dimensional-printed collagen/chitosan/secretome derived from HUCMSCs scaffolds for efficient neural network reconstruction in canines with traumatic brain injury. Regen Biomater 9:rbac043.

Liu XY, Liang J, Wang Y, Zhong L, Zhao CY, Wei MG, Wang JJ, Sun XZ, Wang KQ, Duan JH, Chen C, Tu Y, Zhang S, Ming D, Li XH (2019) Diffusion tensor imaging predicting neurological repair of spinal cord injury with transplanting collagen/chitosan scaffold binding bFGF. J Mater Sci Mater Med 30:123.

Liu XY, Wei MG, Liang J, Xu HH, Wang JJ, Wang J, Yang XP, Lv FF, Wang KQ, Duan JH, Tu Y, Zhang S, Chen C, Li XH (2020) Injury-preconditioning secretome of umbilical cord mesenchymal stem cells amplified the neurogenesis and cognitive recovery after severe traumatic brain injury in rats. J Neurochem 153:230-251.

Liu XY, Chen C, Xu HH, Zhang YS, Zhong L, Hu N, Jia XL, Wang YW, Zhong KH, Liu C, Zhu X, Ming D, Li XH (2021) Integrated printed BDNF/collagen/chitosan scaffolds with low temperature extrusion 3D printer accelerated neural regeneration after spinal cord injury. Regen Biomater 8:rbab047.

Llorens-Martin M, Torres-Aleman I, Trejo JL (2009) Mechanisms mediating brain plasticity: IGF1 and adult hippocampal neurogenesis. Neuroscientist 15:134-148.

Luo Z, Du H (2020) Prospect of different types of magnetic nanoparticles in stem cell therapy. Stem Cell Rev Rep 16:675-683.

Ma C, Kuzma ML, Bai X, Yang J (2019a) Biomaterial-based metabolic regulation in regenerative engineering. Adv Sci (Weinh) 6:1900819.

Ma K, Xu H, Zhang J, Zhao F, Liang H, Sun H, Li P, Zhang S, Wang R, Chen X (2019b) Insulin-like growth factor-1 enhances neuroprotective effects of neural stem cell exosomes after spinal cord injury via an miR-219a-2-3p/YY1 mechanism. Aging (Albany NY) 11:12278-12294.

Nakamura Y, Miyaki S, Ishitobi H, Matsuyama S, Nakasa T, Kamei N, Akimoto T, Higashi Y, Ochi M (2015) Mesenchymal-stem-cell-derived exosomes accelerate skeletal muscle regeneration. FEBS Lett 589:1257-1265.

National Research Council (2011) Guide for the Care and Use of Laboratory Animals, 8th ed. Washington, DC: The National Academies Press.

Othman FA, Tan SC (2020) Preconditioning strategies to enhance neural stem cell-based therapy for ischemic stroke. Brain Sci 10:893.

Paxinos G, Watson C (2006) The rat brain in stereotaxic coordinates, 6th ed. San Diego, CA: Academic Press-Elsevier.

Sharma P, Mesci P, Carromeu C, McClatchy DR, Schiapparelli L, Yates JR, 3rd, Muotri AR, Cline HT (2019) Exosomes regulate neurogenesis and circuit assembly. Proc Natl Acad Sci U S A 116:16086-16094.

Shen WB, Plachez C, Tsymbalyuk O, Tsymbalyuk N, Xu S, Smith AM, Michel SL, Yarnell D, Mullins R, Gullapalli RP, Puche A, Simard JM, Fishman PS, Yarowsky P (2016) Cell-based therapy in TBI: magnetic retention of neural stem cells in vivo. Cell Transplant 25:1085-1099.

Stevanato L, Thanabalasundaram L, Vysokov N, Sinden JD (2016) Investigation of content, stoichiometry and transfer of miRNA from human neural stem cell line derived exosomes. PLoS One 11:e0146353.

Stocchetti N, Carbonara M, Citerio G, Ercole A, Skrifvars MB, Smielewski P, Zoerle T, Menon DK (2017) Severe traumatic brain injury: targeted management in the intensive care unit. Lancet Neurol 16:452-464.

Sun Y, Yang C, Zhu X, Wang JJ, Liu XY, Yang XP, An XW, Liang J, Dong HJ, Jiang W, Chen C, Wang ZG, Sun HT, Tu Y, Zhang S, Chen F, Li XH (2019) 3D printing collagen/chitosan scaffold ameliorated axon regeneration and neurological recovery after spinal cord injury. J Biomed Mater Res A 107:1898-1908.

Suo H, Zhang J, Xu M, Wang L (2021) Low-temperature 3D printing of collagen and chitosan composite for tissue engineering. Mater Sci Eng C Mater Biol Appl 123:111963.

Szarka N, Szellar D, Kiss S, Farkas N, Szakacs Z, Czigler A, Ungvari Z, Hegyi P, Buki A, Toth P (2021) Effect of growth hormone on neuropsychological outcomes and quality of life of patients with traumatic brain injury: a systematic review. J Neurotrauma 38:1467-1483.

Tajiri N, Duncan K, Antoine A, Pabon M, Acosta SA, de la Pena I, Hernadez-Ontiveros DG, Shinozuka K, Ishikawa H, Kaneko Y, Yankee E, McGrogan M, Case C, Borlongan CV (2014) Stem cell-paved biobridge facilitates neural repair in traumatic brain injury. Front Syst Neurosci 8:116.

Tan HX, Del Borgo MP, Aguilar MI, Forsythe JS, Taylor JM, Crack PJ (2020) The use of bioactive matrices in regenerative therapies for traumatic brain injury. Acta Biomater 102:1-12.

Tenuta M, Carlomagno F, Cangiano B, Kanakis G, Pozza C, Sbardella E, Isidori AM, Krausz C, Gianfrilli D (2021) Somatotropic-Testicular Axis: A crosstalk between GH/IGF-I and gonadal hormones during development, transition, and adult age. Andrology 9:168-184.

Verstappen K, Aquarius R, Klymov A, Wever KE, Damveld L, Leeuwenburgh SCG, Bartels RHMA, Hooijmans CR, Walboomers XF (2022) Systematic evaluation of spinal cord injury animal models in the field of biomaterials. Tissue Eng Part B Rev doi: 10.1089/ten.TEB.2021.0194.

Vogel A, Upadhya R, Shetty AK (2018) Neural stem cell derived extracellular vesicles: Attributes and prospects for treating neurodegenerative disorders. EBioMedicine 38:273-282.

Wang J, Wang J, Li X, Shu K (2022) Cell-derived exosomes as therapeutic strategies and exosome-derived microRNAs as biomarkers for traumatic brain injury. J Clin Med 11:3223.

Wiles MD (2022) Management of traumatic brain injury: a narrative review of current evidence. Anaesthesia 77 Suppl 1:102-112.

Zhang J, Liu X, Ma K, Chen M, Xu H, Niu X, Gu H, Wang R, Chen X, Sun H (2021a) Collagen/heparin scaffold combined with vascular endothelial growth factor promotes the repair of neurological function in rats with traumatic brain injury. Biomater Sci 9:745-764.

Zhang J, Wang RJ, Chen M, Liu XY, Ma K, Xu HY, Deng WS, Ye YC, Li WX, Chen XY, Sun HT (2021b) Collagen/heparan sulfate porous scaffolds loaded with neural stem cells improve neurological function in a rat model of traumatic brain injury. Neural Regen Res 16:1068-1077.

Zhang L, Fan C, Hao W, Zhuang Y, Liu X, Zhao Y, Chen B, Xiao Z, Chen Y, Dai J (2021c) NSCs migration promoted and drug delivered exosomes-collagen scaffold via a bio-specific peptide for one-step spinal cord injury repair. Adv Healthc Mater 10:e2001896.

Zhao H, Yang L, Baddour J, Achreja A, Bernard V, Moss T, Marini JC, Tudawe T, Seviour EG, San Lucas FA, Alvarez H, Gupta S, Maiti SN, Cooper L, Peehl D, Ram PT, Maitra A, Nagrath D (2016) Tumor microenvironment derived exosomes pleiotropically modulate cancer cell metabolism. Elife 5:e10250.

Zipser CM, Cragg JJ, Guest JD, Fehlings MG, Jutzeler CR, Anderson AJ, Curt A (2022) Cell-based and stem-cell-based treatments for spinal cord injury: evidence from clinical trials. Lancet Neurol 21:659-670.

C-Editor: Zhao M; S-Editor: Li CH; L-Editors: Li CH, Song LP; T-Editor: Jia Y